Computational Techniques and Validation of Blood Flow Simulation

LUISA SOUSA*, CATARINA CASTRO*, CARLOS ANTÓNIO*, RUI CHAVES**
*Mechanical Department and IDMEC, **IDMEC - Instituto de Engenharia Mecânica
Universidade do Porto
R. Dr. Roberto Frias, 4200-465 Porto
PORTUGAL
lcsousa@fe.up.pt, https://www.fe.up.pt/~lcsousa

Abstract: - Plaque formation leading to stenosis and occlusion of arterial blood vessels causes altered flow conditions, such as separation and flow-reversal zones and plays an important role in the development of arterial diseases. Computational simulations of blood flow can help to understand the hemodynamics in blood vessels and to predict the outcomes of surgeries. The paper presents a three dimensional numerical method of steady and pulsatile blood flow simulation in arteries by the finite element method. In this study the biochemical and mechanical interactions between blood and vascular tissue are neglected and no-slip boundary conditions are considered at the artery wall. Velocity field is calculated by a mixed method using a smoothed deviatoric stress field in order to obtain an improvement of the finite element method performance. Stabilized finite element formulations to properly treat incompressible and high Reynolds number flows are presented. Velocity and wall shear stress fields are visualized for a better understanding of flow characteristics such as distributions of the flow pattern, stagnation flow and recirculation zones. Simulated results are compared and validated with literature data obtained from ultrasound measurements.

Key-Words: - Blood flow, Finite Element Method, mixed methods, upwinding techniques

1 Introduction

The accumulation of plaques on an artery wall is a progressive disease induced by local irregular flow field. Although clinical symptoms of this disease become evident when the stenosis percentage is around 70%, modifications of the flow characteristics such as separation and flow-reversal zones, occur at milder degrees of stenosis. It is well established that once a mild stenosis is formed in the artery, biomechanical parameters resulting from the altered blood flow and stress distribution in the arterial wall contribute to further progression of the disease [1-3]. Upstream from a stenosis high shear stress exists while downstream regions are exposed to low shear stress and flow separation. Fluid shear stresses, flow reversal and stagnation zones induce vascular oxidation stress, pro-inflammatory states and arterial internal thickening.

Hemodynamic finite element simulation studies have been frequently used to gain a better understanding of functional, diagnostic and therapeutic aspects of the blood flow [4-13].

The mechanics of blood flow in arteries plays an important role in the health of individuals and its study represents a central issue of the vascular research. A detailed understanding of local hemodynamic environment, influence of wall modifications on flow patterns and long-term adaptations of the vascular wall provides an effective way of obtaining detailed flow patterns associated with diseases that can have useful clinical applications, especially in the design of devices that mimic or alter blood flow as in reconstruction and revascularization operations [14-16].

Flow visualization techniques and non-invasive medical imaging data acquisition such as computed tomography, angiography or magnetic resonance imaging, make feasible to construct three dimensional models of blood vessels. Colour Doppler ultrasound provides real-time cross-sectional images of endovascular structure and measuring techniques have improved to provide accurate information on the flow fields. Validated computational fluid dynamics (CFD) models using data obtained by these currently available measurement techniques [11, 12, 17-19] can be very valuable in the early detection of vessels at risk and prediction of future disease progression.

The arterial wall is a composite of three layers, each containing different amounts of elastin, collagen, vascular smooth muscle cells and extracellular matrix. Endothelial cells form a monolayer that constitutes the primary interface between the bloodstream and all extravascular tissue. The endothelial cell layer acts mostly as a wall sensing and responding to shear stress and hemodynamic forces plays an important role in

stimulating vascular remodelling and probable development of lesions. Experimental data show that arteries in regions of denuded endothelium lose the capacity to adapt their diameter in response to modifications of blood flow. In diseased vessels which are often the subject of interest, the arteries are less compliant, wall motion is reduced and in most approximations the assumption of rigid vessel flow is reasonable.

Blood is a suspension of different particles in an aqueous polymer solution, the plasma. About 45% volume consists of formed elements, mostly red blood cells, and about 55% of plasma. Due to its complex nature blood is a non-Newtonian fluid. In large and medium size vessels, blood is usually modelled as a Newtonian liquid. However in smaller vessels blood is a complex rheological mixture showing several non-Newtonian properties, as shear-thinning or viscoelasticity [5,10]. The temperature and the presence of pathological conditions may also contribute to non-Newtonian behaviour.

For the steady flow case Himeno [10] showed that the non-Newtonian effect is small except for the peak shear stress and that for the pulsatile case the Newtonian effect in the artery is small and negligible. Perktold and co-workers [5] examined non-Newtonian viscosity models in carotid artery bifurcation and although the Newtonian assumption yields no change in the essential flow characteristics they concluded that predicted shear stress magnitude resulted in differences on the order of 10% as compared with Newtonian models.

The objective of this paper is to report the development of two finite element approaches of a three dimensional numerical simulation system for the clinical study of arterial blood flow under steady and pulsatile conditions. Considering blood flow an incompressible non-Newtonian flow, the fluid flow is governed by the incompressible Navier-Stokes equations. There are two potential sources of numerical instability in the Galerkin finite element solution of these equations. The first is due to the numerical treatment of the saddle-point problem arising from the variational formulation of the incompressible flow equations. The second difficulty is related to the solution of a convection-dominated transport problem by the standard Galerkin method which leads to spurious node-to-node oscillations; this problem requires the use of stabilized finite element formulations to properly treat high Reynolds number flows. Some of the approaches for calculating 3D numerical solutions are presented in this study aiming numerical stability and computer time reduction.

The developed code is validated using experimental and numerical data obtained from the literature.

2 Problem Formulation

A number of important phenomena in fluid mechanics are described by the Navier-Stokes equations. They are a statement of the dynamical effect of the externally applied forces and the internal forces due to pressure and viscosity of the fluid. A peculiar feature of blood flow is the pulsatility induced by the periodic contractive and relaxing motion of the heart. The time dependent flow of a fluid is governed by the mass, momentum and energy conservation equations; the blood is a viscous incompressible fluid, and under isothermal conditions the Navier-Stokes equations, for blood flow are given as:

$$\rho\left(\frac{\partial \mathbf{u}}{\partial t}+\left(\mathbf{u}.\nabla\right)\mathbf{u}\right)=\nabla.\boldsymbol{\sigma}+\mathbf{f}$$
$$\nabla.\mathbf{u}=0 \tag{1}$$

where $\mathbf{u}$ and $\boldsymbol{\sigma}$ are the velocity and the stress fields, ρ the blood density and $\mathbf{f}$ the volume force per unit mass of fluid. The components of the stress tensor are defined by the Stokes' law:

$$\boldsymbol{\sigma}=-p\mathbf{I}+2\mu\boldsymbol{\varepsilon}(\mathbf{u})=-p\mathbf{I}+\mathbf{S} \tag{2}$$

where p is the pressure, $\mathbf{I}$ the unit tensor, μ the dynamical viscosity, $\boldsymbol{\varepsilon}(\mathbf{u})$ the strain rate tensor and $\mathbf{S}$ the deviatoric stress. Considering a three dimensional formulation, momentum and mass conservation equations from Eq. (1) become:

$$\rho\left(\frac{\partial u_i}{\partial t}+u_j\frac{\partial u_i}{\partial x_j}\right)-\mu\nabla^2\mathbf{u}+\frac{\partial p}{\partial x_i}=\mathbf{f}\ or\ \boldsymbol{\mathcal{L}}(\mathbf{u})-\mathbf{f}=0$$
$$\frac{\partial u_i}{\partial x_i}=0 \qquad i,j=1,2,3 \tag{3}$$

This equation system, Eq. (3) can be solved for the velocity and the pressure given appropriate boundary and initial conditions. In this study the biochemical and mechanical interactions between blood and vascular tissue are neglected. The innermost lining of the arterial wall in contact with the blood is a layer of firmly attached endothelial cells and it appears to be reasonable to assume no slip at the interface with the rigid vessel wall; at the

flow entrance Dirichelet boundary conditions for all points are considered prescribing the time dependent value $\mathbf{u}_D$ for the velocity on the portion Γ_D of the boundary:

$$\mathbf{u}(\mathbf{x},t) = \mathbf{u}_D(\mathbf{x},t), \quad \mathbf{x} \in \Gamma_D \tag{4}$$

The condition describing surface traction force $\mathbf{h}$ at an outflow boundary Γ_N can be described mathematically by the condition:

$$\left(-p\delta_{ij} + \mu\left(\frac{\partial u_i}{\partial x_j} + \frac{\partial u_j}{\partial x_j} \right) \right) n_j = h_i \quad i, j = 1,2,3 \tag{5}$$

where n_j are the components of the outward pointing unit vector at the outflow boundary and δ_{ij} is the Kronecker delta.

3 Finite element models

The finite element method (FEM) is a mathematical technique for obtaining approximate numerical solution of the physical phenomena subject to initial and boundary conditions. The accuracy of numerical solutions depends on the selected formulation. Two different finite element models of the Navier-Stokes equations are considered in this work, the mixed model and the penalty finite element model [20]. Further a numerical scheme with a stabilization technique to avoid numerical oscillations of the solution is presented, the streamline upwind/Petrov Galerkin method.

3.1 Mixed finite element model

The mixed model is a natural formulation in which the weak forms of Eq. (3) are used to construct the finite element method. The resulting finite element model is termed the velocity-pressure model or mixed model. Developing a Galerkin formulation the weak forms of Eq. (3) results in the following finite element equations:

$$\begin{aligned} &\mathbf{M}\dot{\mathbf{u}} + \mathbf{C}(\mathbf{u})\mathbf{u} + \mathbf{K}\mathbf{u} - \mathbf{Q}\mathbf{p} = \mathbf{F} \\ &\mathbf{Q}^T\mathbf{u} = \mathbf{0} \end{aligned} \tag{6}$$

where the superpose dot represents a time derivative and **M**, **C**, **K** and **Q** are the mass, convection, viscous and gradient matrices, respectively. Considering N the element interpolation functions for the velocity, the vector **F** is given as:

$$\mathbf{F} = \int_e \rho \mathbf{N}\mathbf{f}\, de + \int_{\Gamma_N} \mathbf{N}\mathbf{t}\, d\Gamma \tag{7}$$

where **t** is the traction forces vector on the boundary Γ_N. The resulting equation system is:

$$\mathbf{M}\dot{\mathbf{u}} + \begin{bmatrix} \mathbf{C}+\mathbf{K} & -\mathbf{Q} \\ \mathbf{Q}^T & \mathbf{0} \end{bmatrix} \begin{Bmatrix} \mathbf{u} \\ \mathbf{p} \end{Bmatrix} = \begin{Bmatrix} \mathbf{F} \\ \mathbf{0} \end{Bmatrix} \tag{8}$$

The above partitioned system, Eq. (8), with a null submatrix could in principle be solved in several ways. However, a numerical problem results from the incompressibility condition and it can be asked under which conditions it can be safely solved. In simple terms, we want to obtain, in the linear space U of all admissible solutions, the velocity field **u** belonging to a subspace, $I^h \subset U$ associated to the space of incompressible deformations. This subspace is given as:

$$I^h = \left\{ \mathbf{u}^h \in U^h : \mathbf{Q}\mathbf{u}^h = \mathbf{0} \right\} \tag{9}$$

The solution I^h should then lie on the null space of **Q** that must be zero.

The numerical problem described above is eliminated by proper choice of finite element spaces for the velocity and pressure fields; in other words the evaluation of the integrals for the stiffness matrix where velocity and pressure interpolations appear must satisfy the Babuska-Brezzi compatibility condition the so called LBB condition [21-23] that states: velocity and pressure spaces can not be chosen arbitrarily and a link between them is necessary.

Considering a 3D analysis hexahedral meshes often provide the best quality solution as errors due to numerical diffusion are reduced whenever a good alignment between mesh edges and flow exists [24]; in this work a spatial discretization with isoparametric brick elements of low order with trilinear approximation for the velocity components and element constant pressure is adopted:

$$\mathbf{u}(\mathbf{x},t) = \sum_{i=1}^{8} N_i(\mathbf{x}) u_i(t) \quad \text{and} \quad p(t) = L p_c(t) \tag{10}$$

where L are pressure interpolation functions and u_i and p_c are the unknown element velocity node and the pressure element center values, respectively.

Zienkiewicz [25] shows that mixed methods are able to satisfy the incompressibility constraint with

a small number of iterations. These methods allow obtaining smoother velocity and stress fields. They are an inexpensive improvement of the finite element method performance and further faster convergence is achieved. When 3D simulations are considered and consequently computation time would become limitative the consideration of these methods is compulsory.

The deviatoric stress in Eq. (2) can be expressed as a linear combination of the nodal deviatoric stress $\hat{\mathbf{S}}$ obtained by local or global smoothing and the deviatoric stress field $\mathbf{S}$ [25]:

$$\mathbf{S}^{*} = -\gamma\,\hat{\mathbf{S}} + (1+\gamma)\mathbf{S} \quad \text{where } \hat{\mathbf{S}} = N_s\mathbf{S} \tag{11}$$

Substituting in Eq. (2) the weak form of Eq. (3) becomes:

$$\mathbf{M}\dot{\mathbf{u}} + \begin{bmatrix} \mathbf{Q}_1 & \mathbf{Q}_2 & \mathbf{0} \\ \mathbf{Q}_3 & \mathbf{C}+\mathbf{K} & -\mathbf{Q} \\ \mathbf{Q}^T & \mathbf{0} & \mathbf{0} \end{bmatrix} \begin{Bmatrix} \mathbf{S} \\ \mathbf{u} \\ \mathbf{p} \end{Bmatrix} = \begin{Bmatrix} \mathbf{0} \\ \mathbf{F} \\ \mathbf{0} \end{Bmatrix} \tag{12}$$

where

$$\mathbf{Q}_1 = \beta\int_e \mathbf{N_s^T N_s}\,d_e,\ \mathbf{Q}_2 = -\beta\int_e \mu\mathbf{N_s^T B}\,d_e \quad \text{and } \mathbf{Q}_3 = -\beta\int_e \mathbf{B^T N_s}\,d_e \tag{13}$$

and $\mathbf{B}$ is the rate deformation matrix.

In this paper the numerical procedure for the transient non-Newton inelastic Navier-Stokes equations uses the Galerkin-finite element method with implicit time discretization. At each time step Picard iteration is applied to linearize the non-linear convection and diffusion terms; the method is based on a pressure correction [5, 6, 20]. The essential steps of the algorithm at a time or iteration are:

1. Calculation of an auxiliary velocity field $\mathbf{u}^{n+1/2,m+1}$ from the equations of motion using known pressure values from the previous time *n* step or previous iteration step *m* ;
2. Calculation of the pressure correction using lumped mass matrix:

$$\mathbf{Q^T M_d^{-1}\,Q}\,q^{n+1,m+1} = \frac{1}{\Delta t}\mathbf{Q^T u}^{n+1/2,m+1} \tag{14}$$

where $\mathbf{M}_d$ is the lumped matrix;

3. Pressure updating: $p^{n+1,m+1} = p^{n+1,m} + q^{n+1,m+1}$;
4. Calculation of the divergence free velocity field:

$$\mathbf{u}^{n+1,m+1} = \mathbf{u}^{n+1/2,m+1} + \Delta t\,\mathbf{M}_d^{-1}\mathbf{Q}q^{n+1,m+1} \tag{15}$$

5. Calculation of the apparent viscosity.

This method, developed for obtaining a divergence-free velocity field, has been based on Chorin's method [26] and validated by other authors [5, 6]. It will be considered to reproduce flow in a human carotid bifurcation under pulsatile conditions.

3.2 Penalty finite element model

The incompressibility constraint given by $\varepsilon_{ii} = 0$ is difficult to implement due to the zero divergence condition for the velocity field. However the incompressibility problem may be stated as a constrained minimization of a functional. The penalty function method allows us to reformulate a problem with constraints as one without constraints [21-23]. Using the penalty function method proposed by Courant [27], the problem is transformed into the minimization of the unconstrained augmented functional:

$$\pi(\mathbf{u}) = \pi(\mathbf{u}) + \lambda\int_V \left(\varepsilon_{ii}\left(\mathbf{u}\right)\right)^2 \mathrm{d}V \tag{16}$$

Considering the pseudo-constitutive relation for the incompressibility constraint the second set of Eq. (3) is replaced by:

$$\nabla.\mathbf{u} = -p/\lambda \tag{17}$$

where λ is the penalty parameter. If λ is too small compressibility and pressure errors will occur and an excessively large value may result in numerical ill conditioning; generally λ is assigned to $\lambda = \beta\mu$ being β a constant of order 10^7 for double precision calculations. The second set of Eq. (3) is eliminated and the Navier-Stokes equations become:

$$\mathbf{M}\dot{\mathbf{u}} + \left(\mathbf{C}+\mathbf{K}+\mathbf{K}^{\lambda}\right)\mathbf{u} = \mathbf{F} \tag{18}$$

where $\mathbf{K}^{\lambda}$ is the so-called penalty matrix:

$$\mathbf{K}^{\lambda} = \lambda\mathbf{Q}\mathbf{M}^{p}\mathbf{Q}^{\mathbf{t}} \quad \textit{and} \quad \mathbf{M}^{p}\mathbf{p} = \lambda\mathbf{Q}^{\mathbf{t}}\mathbf{u} \quad \textit{with} \quad M_{ij}^{p} = \int_e L_i L_j\,de \tag{19}$$

Under such conditions the pressure is eliminated as a field variable since it can be recovered by the approximation given in the above equation,

$\mathbf{p} = \lambda(\mathbf{M}^p)^{-1}\mathbf{Q}^t\mathbf{u}$ with a known velocity field. The penalty finite element method is often applied to numerical discretization since it gives a reduction of the size system of equations.

If the standard Galerkin formulation is applied it is necessary to use compatible spaces for the velocity and the pressure in order to satisfy the LBB stability condition. This often excludes the use of equal order interpolation functions for both fields. In order to avoid oscillatory results the numerical problem is eliminated by proper evaluation of the integrals for the stiffness matrix where penalty terms are calculated using a numerical integration rule of an order less than that required to integrate them exactly, the well known reduced integration.

3.3 Streamline upwind/Petrov Galerkin method

In a Galerkin formulation there is no doubt that the most difficult problem arises because of the nonlinear convective term in Eq. (3). In blood flow high Reynolds numbers, dynamical instabilities and turbulence appear and loss of unicity of solution is caused by the apparently innocent convective term. It can be removed by mesh and time step refinement which clearly undermine the practical utility of the method. On the other hand a numerical scheme with a stabilization technique can be used in order to avoid oscillations in the numerical solution.

In two or three dimensions the convection is only active in the direction of the resultant element velocity **U** and the corrective diffusion introduced by upwinding should be anisotropic with a coefficient different from zero only in the direction of the velocity resultant. One appropriate technique to solve these problems is the Streamline upwind/Petrov Galerkin method, SUPG-method [28-32]. The goal of this technique is the elimination of the instability problems of the Galerkin formulation by introducing an artificial dissipation. The method uses modified weighting functions, W_a, defined as a function of **U** and h, element velocity and characteristic length, respectively, and the grid Peclet number Pe. Considering steady blood flow [32] weighting functions are defined as:

$$W_a = N_a + \alpha W_a^* = N_a + \frac{\alpha h}{2}\frac{U_j}{\|\mathbf{U}\|}\frac{\partial N_a}{\partial x_j} \qquad (20)$$
$$j = 1,2,3; \quad a = 1,\ldots Nnode$$

Here α is determined for each element as follows:

$$\alpha = \alpha_{opt} = \coth Pe - \frac{1}{Pe}, \quad Pe = \frac{\|\mathbf{U}\|h}{2k} \qquad (21)$$
$$with \quad \|\mathbf{U}\| = \sqrt{U_i U_i}$$

where k is the diffusion coefficient. Using the weighting functions defined above the SUPG method is computed from the weighted residual form:

$$\int_\Omega \left(N_a + \frac{\alpha h}{2}\frac{U_i}{\|\mathbf{U}\|}\frac{\partial N_a}{\partial x_i} \right)\left(\mathcal{L}(\mathbf{u}) - \mathbf{F}\right) d\Omega = 0$$
$$\int_\Omega \frac{\partial u_i}{\partial x_i} = 0, \qquad i = 1,2,3 \qquad (22)$$

For a transient analysis Petrov-Galerkin weighting functions are given as [32]:

$$W_i = N_a + \frac{\Delta t U_i}{2}\frac{\partial N_a}{\partial x_i} \qquad (23)$$

excluding the time derivative terms to which standard Galerkin weighting functions are applied. As the LBB stability condition is satisfied by the different order interpolation for the velocity and pressure, the second equation of the above system does not need stabilization. The SUPG-method produces a substantial increase in accuracy as stabilizing artificial diffusivity is added only in the direction of the streamlines and crosswind diffusion effects are avoided [32].

The resulting system of nonlinear equations is characterized by a non-symmetric matrix, and a special solver is adopted in order to reduce the bandwidth and the storage of the sparse system matrix; in addition the Skyline method is used to some improvement of the Gauss elimination.

4 Numerical Results

Numerical solutions for velocity and stress fields are validated against published experimental data obtained by Doppler ultrasound measurements. The first example is the simulation of a three-dimensional eccentric stenotic model presented by Lisong Ai [12]. Computer simulation is carried out under steady flow conditions using the penalty method. The second one is the study of blood flow in a human carotid bifurcation [11]. The mixed method described in section 3.1 is applied to calculate the pulsatile flow simulation. In both cases numerical results for the flow velocity field are

presented and compared with numerical and ultrasound data.

4.1 An eccentric arterial stenotic model

Validation of the developed penalty method is made considering a 3D eccentric stenotic model [12]. The Navier-stokes equations were solved for laminar, incompressible and Newtonian flow. The numerical simulation was performed considering the fluid as a homogeneous Newtonian fluid with a dynamic viscosity equal to 0.00345 kg/(m s).

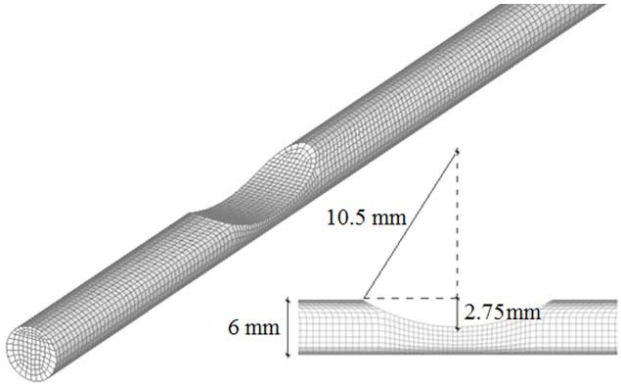

Fig. 1. Geometry and finite element mesh of the stenotic model.

The geometric characteristics of the stenosis 3D model are presented in Fig. 1. In the finite element simulation the tube was set to 216 mm length with an entrance and an exit circular cross section of 6 mm diameter. The stenosis with a 21 mm length mimics the eccentric one presented by Ai [12]. The center of the stenosis was located 40 mm downstream from the inlet in order to allow a fully developed flow. The stenosis with a radius of 10.5 mm was placed at the middle of the tube. The boundary conditions are a specified parabolic inlet velocity corresponding to a flow rate equal to 150 ml/min, no slip at the tube wall and traction free at the exit. Computer simulation is carried out under steady flow conditions. The finite element mesh was built using 9978 elements and 12096 nodes. The mesh is fine enough to generate good quality information to characterize the large fluid velocity gradients.

Fig. 2 shows the axial velocity in the symmetric plane, velocity profiles in some sections on the stenosed region and wall shear stress field. The developed code was able to detect flow reversal corresponding to a recirculation region downstream from the stenosis. Along the throat, the highest velocity magnitude region and the highest magnitude of shear stresses are found. The numerical findings on flow separation zone downstream from the stenosis agree well in location with previously published results [12].

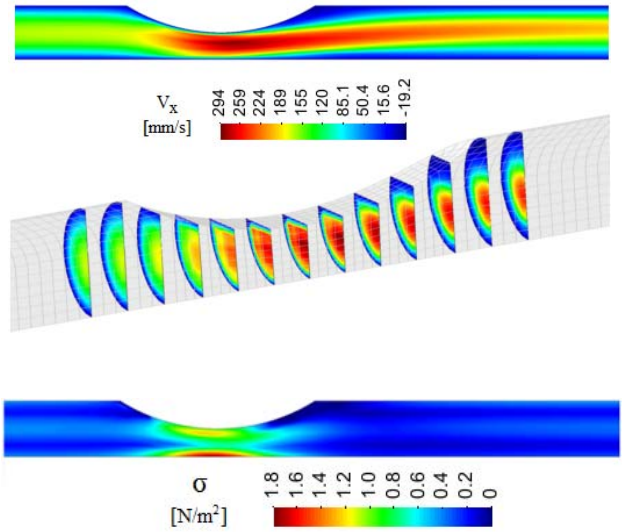

Fig. 2. Velocity field and wall shear stress of the stenosis.

Comparison between computed and published axial velocity profiles at three different locations is presented in Figs. 3, 4 and 5. It can be seen that upstream and downstream from the stenosis, the presented numerical results fit the experimental data and the numerical Fluent code results obtained by Lisong Ai [12]. Upstream from the stenosis our simulated results overlap much better the Doppler measured values than the Fluent results. At the throat our simulated results coincide with the Fluent data. According to Ai [12] discrepancy between numerical and experimental data is due to the flow disturbance introduced by ultrasound measurement.

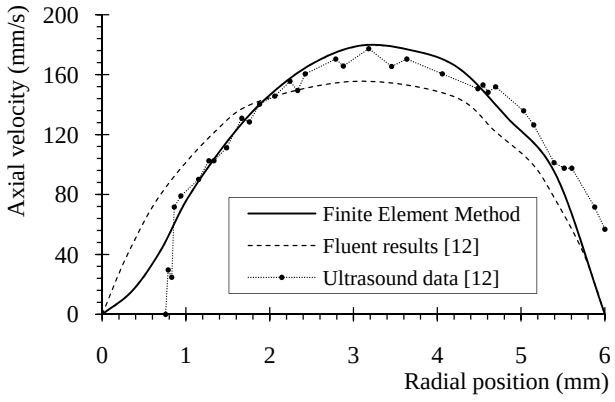

Fig. 3. Velocity profile upstream the stenosis.

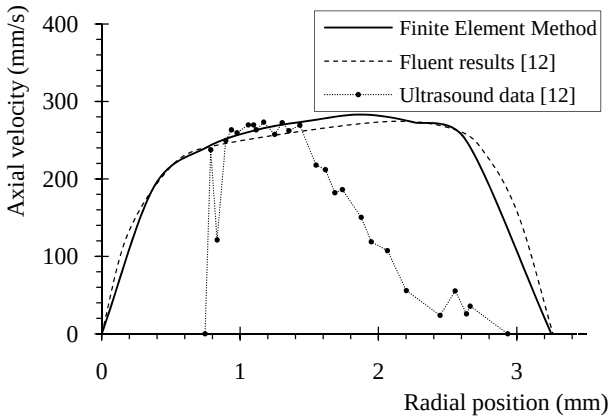

Fig. 4. Velocity profile at the throat of the stenosis.

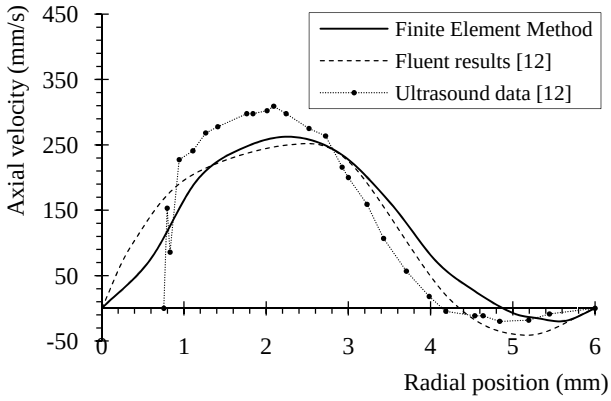

Fig. 5. Velocity profile downstream the stenosis.

Downstream the stenosis our developed code predicts a magnitude for the velocities in agreement with the ultrasound data, although the reversal location is closer to the vessel wall. Observed differences are within the uncertainty location of the selected section.

4.2 Carotid artery bifurcation

Carotid bifurcation is prone to atherosclerotic lesions but the precise hemodynamic determinants of atherosclerotic disease are not yet completely understood. In this example a study of blood flow in a human carotid bifurcation is considered using the mixed method for the pulsatile flow simulation. The model for the carotid bifurcation will consider rigid walls and traction free outflow. Results will be compared to clinical data and calculations presented by Maurits et al. [11].

The geometry of the carotid bifurcation under study is shown in Fig. 6 and follows as much as possible the 3D surface markers to quantify common carotid artery (CCA), external carotid artery (ECA), internal carotid artery (ICA) and superior thyroid artery (STA) and the connections between segments [11]. Numerical simulation is performed considering pulsatile blood flow with time dependent parabolic inlet velocity and maximum value given by ultrasound measurements at the distal common carotid artery section (DCCA), placed 2 cm before bifurcation. Fig. 7 describes the flow wave form for one cardiac cycle of period equal to one second.

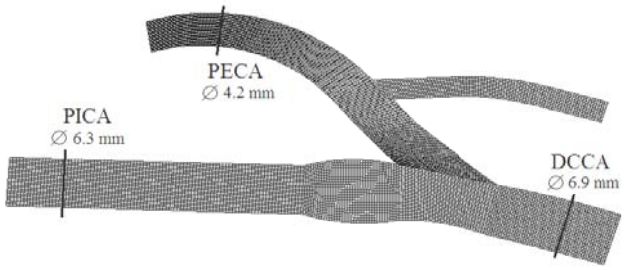

Fig. 6. Geometry and finite element mesh of the carotid bifurcation.

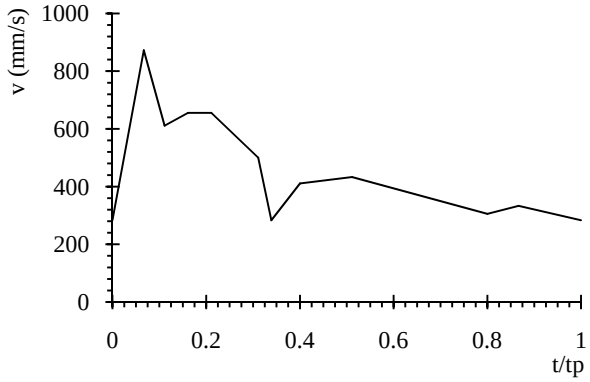

Fig. 7. Flow pulse waveform at DCCA [11].

At the rigid artery wall the no slip condition is applied (**u** = 0). The conditions describing vanishing normal and tangential force of Eq. (5) cannot be applied simultaneously at ICA and ECA outflow boundaries [5, 6]. The flow simulation is carried out in two steps. In the first calculation step, 65% of the common carotid artery flow is assumed at the internal carotid outlet, according to experimental observation [11], and the condition of zero surface traction force is applied at the external carotid outflow boundary. During the second calculation step, which is the actual calculation step, the condition of zero surface traction force is applied at the internal carotid outflow boundary, while at the external carotid outflow boundary the results for the velocity profiles from the first step are used. In both simulations traction free condition is assumed at the thyroid artery outlet.

Calculated velocity fields for two positions are presented and compared with previously published data. The first, the proximal external carotid artery (PECA) corresponds to the most proximal point at the external carotid artery without flow disturbance from bifurcation, and the second one, the proximal internal carotid artery (PICA) is situated 3 cm after the bulbus at the internal carotid artery.

In Fig. 8 the flow wave calculated during one cardiac cycle at PECA section is shown. Superposed on the FEM results similar published wave forms are displayed using a finite-volume discretization with rigid walls for Model A and elastic walls with traction-free outflow for Model C and with positive peripheral resistance for Model D [11]. FEM results are within the interval of variation considering those different models. For all models the PECA flow wave reflects the inlet flow impulse representative of the mechanical heart action as given by the flow pulse waveform of DCCA at Fig. 7.

For the FEM model the maximum and minimum values for the velocity are equal to 618 and 142 mm/s respectively, while maximum velocity value measured by ultrasound [11] is equal to 620 mm/s and the minimum 80 mm/s. It is interesting to notice that the ultrasound measured systolic velocity at PECA [11] is similar to our FEM calculations and the ultrasound measured diastolic velocity is lower. The developed FEM model simulates rather well the systolic velocities at PECA but overestimates the diastolic ones. In fact, our diastolic velocity at PECA is very close to the time-averaged mean in vivo measurement velocity value of 140 mm/s [11].

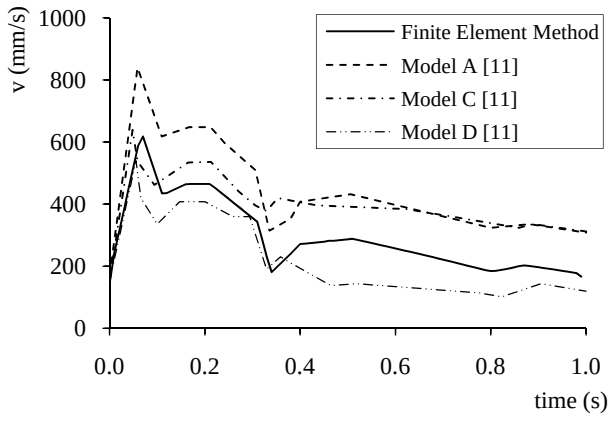

Fig. 8. Flow wave form at PECA: calculated values with FEM and Maurits models A, C and D [11].

Calculated velocity profiles at PICA and PECA representative of different cardiac cycles instants are shown in Figs. 9 to 12. At all cases results are comparable with those obtained numerically by Maurits model D and since model D calculates different systolic and diastolic vessel diameters the profiles were fitted accordingly. Like in literature data, profiles at PECA and PICA are non symmetric with maximum velocity skewed towards the flow divider wall. As referenced in the literature it can be due to the carotid branch curvature.

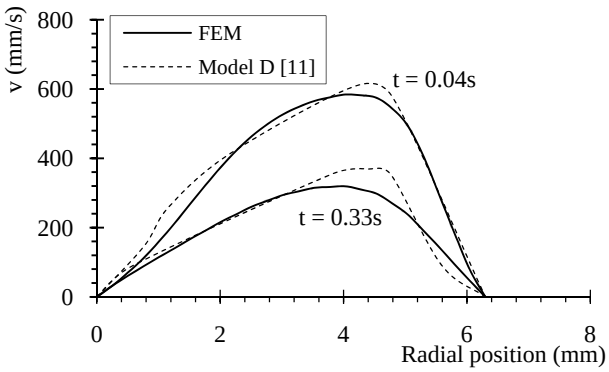

Fig. 9. Comparison of calculated velocity profiles with FEM model and model D [11] at PICA for t=0.04 s and t=0.33 s.

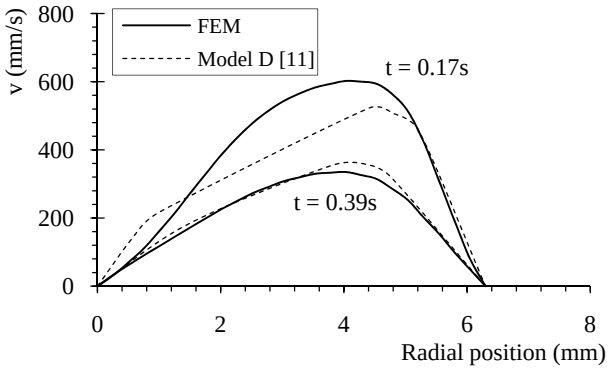

Fig. 10. Comparison of calculated velocity profiles with FEM model and model D [11] at PICA for t=0.17 s and t=0.39 s.

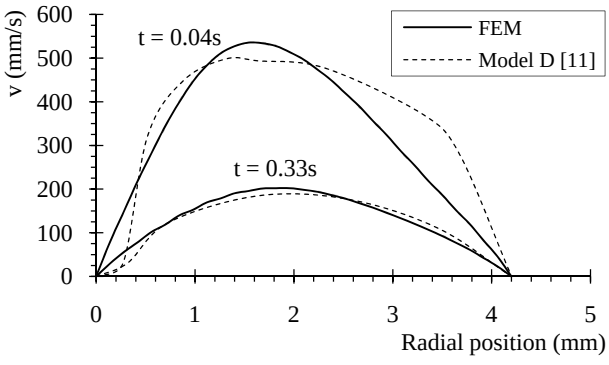

Fig. 11. Comparison of calculated velocity profiles with FEM model and model D [11] at PECA for t=0.04 s and t=0.33 s.

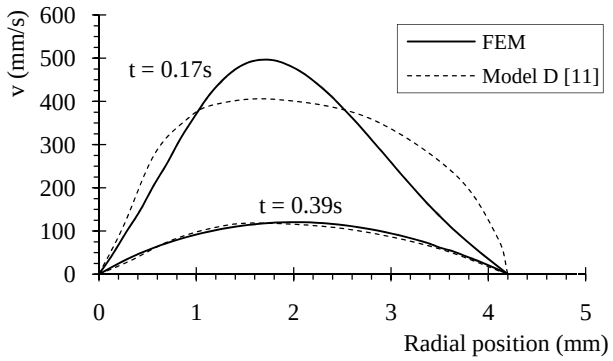

Fig. 12. Comparison of calculated velocity profiles with FEM model and model D [11] at PECA for t=0.17 s and t= 0.39 s.

At the beginning of the cardiac cycle (t=0.04 s) just before the maximum systolic velocity is reached both PICA and PECA velocity profiles are similar but at PECA section it can be observed that FEM calculations give a sharper and more parabolic profile. During systolic flow deceleration (t=0.17 s) the FEM velocity profiles suggest higher maximum velocities for both PICA and PECA sections. Close to the minimum diastolic velocity, t=0.33 s and t=0.39 s, both FEM and model D profiles are quite the same.

The observed differences of compared profiles can be explained by the systolic dilatation and diastolic contraction of the arteries.

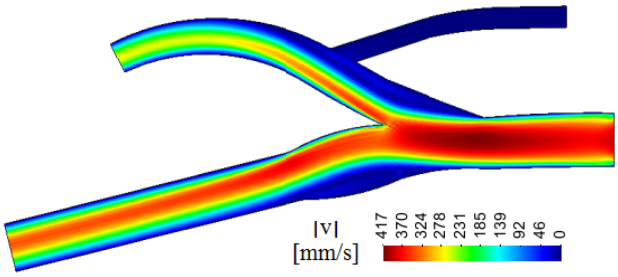

Fig. 13. Velocity field in the symmetric plane of the carotid bifurcation, t=0.40 s.

For the cardiac cycle instant t= 0.40 s velocity field in the symmetric plane of the carotid bifurcation is shown in Fig. 13. It can be observed a strongly skewed axial velocity in the carotid sinus with high velocity gradients at the internal divider wall. The developed code was also able to detect stagnation corresponding to a recirculation region near the outer sinus wall (the wall opposite the divider wall) and also at ECA near the outer wall. In diseased vessels presenting plaque accumulation on the arterial wall, higher velocity gradients would be expected.

5 Conclusion

A computational finite element model for simulating blood flow in arteries is presented. Blood flow is described by the incompressible Navier-Stokes equations and the simulation is carried out under steady and pulsatile conditions. The accuracy and efficiency of the blood simulation is validated comparing with experimental and numerical data. In the first example, simulation of blood flow in a stenosed artery, the developed model was able to identify stagnation and flow reversal downstream from the stenosis in agreement with literature data. For the carotid bifurcation study calculations of the flow field are in good agreement with those reported previously in the literature.

The presented research is helpful for preventing cerebral vascular accidents once the developed code is able to identify stagnation and reversal flow regions in vessels with complex geometry like in stnosed arteries or carotid bifurcation.

Future work should also take in account the influence of compliant walls and consider experimental data collected in clinical practice.

Acknowledgments: This work was partially done in the scope of project PTDC/SAU-BEB/102547/2008, “Blood flow simulation in arterial networks towards application at hospital”, financially supported by FCT – Fundação para a Ciência e a Tecnologia from Portugal.

References:

[1] A. Quarteroni, M. Tuveri and A. Veneziani, Computational Vascular Fluid dynamics: problems, models and methods, *Computer and Visualization in Scienc.*, Vol. 2, 2003, pp. 163-197.

[2] N.R. Madamanchi, A. Vendrov and M.S. Runge, Oxidative stress and vascular disease, *Arterioscler. Thromb. Vasc. Biol.*, Vol. 25, No. 1, 2005, pp. 29-38.

[3] L. Li, R.J. Tatake, K. Natarajan, Y.Taba, G. Garin, C. Tai, E. Leung, J. Surapisitchat, M.Yoshizumi, C. Yan, J. Abe and B.C. Berk, Fluid shear stress inhibits TNF- mediated JNK activation via MEK5-BMK1 in endothelial cells, *Biochem. Biophys. Res. Commun.*, Vol. 370, No. 1, 2008, pp. 159-163.

[4] D.N. Ku, D. P Giddens, C.Z. Zarins and S. Glagov, Pulsatile flow and atherosclerosis in the human carotid bifurcation, *Arteriosclerosis*, Vol. 5, 1985, pp. 293-302.

[5] K. Perktold, M. Resch and H. Florian, Pulsatile Non-Newtonian Flow Characteristics in a Three-Dimensional Human Carotid Bifurcation

Model, *ASME J. Biomech. Eng*., Vol. 113, 1991, pp. 463-475.

[6] K. Perktold and G. Rappitsch, Mathematical modeling of local arterial flow and vessel mechanics. In Crolet, J., Ohayon, R. (eds.) *Computational Methods for Fluid Structure Interaction*, Pitman Research Notes in Mathematics Series, Vol. 306, 1995, pp. 230-245, Longman Scientific and Technical.

[7] H. Huang, V.J. Modi and B.R. Seymour, Fluid mechanics of stenosed arteries, *Int. J. Engng. Sciences*, Vol. 33, 1995, pp. 815-828.

[8] C.A. Taylor, T.J.R. Hughes and C.K. Zarins, Finite element modeling of blood flow in arteries, *Comput. Methods Appl. Mech. Eng*., Vol. 158, 1998, pp. 155-196.

[9] G. Pedrizzetti, K. Perktold, *Cardiovascular Fluid Mechanics*, Springer-Verlag, 2003.

[10] R. Himeno, Blood Flow Simulation toward Actual Application at Hospital, *The 5th Asian Computational Fluid Dynamics*, Korea, 2003.

[11] N.M. Maurits, G.E. Loots and A.E.P. Veldman, The influence of vessel elasticity and peripheral resistance on the carotid artery flow wave form: A CFD model compared to in vivo ultrasound measurements, *Journal of Biomechanics*, Vol. 40, 2007, pp. 427-436.

[12] L. Ai, L. Zhang, W. Dai, C. Hu, K.K. Shung and T.K. Hsiai, Real-time assessment of flow reversal in an eccentric arterial stenotic model, *J. Biomech*., Vol. 43, No. 14, 2010, pp. 2678-2683.

[13] L.C. Sousa, C.F. Castro and C.A.C. António, Blood flow simulation and applications. Book chapter, *Technologies for medical sciences, Series: Lecture Notes in Computational Vision and Biomechanics*, Editors: R.M. Natal Jorge, João Manuel R.S. Tavares, Marcos Pinotti, Alan Slade, Publisher: Springer (in press).

[14] C.M. Su, D. Lee, R. Tran-Son-Tay and W. Shyy, Fluid flow structure in arterial bypass anastomosis, *Journal of Biomechanical Eng.*, Vol. 127, 2005, pp. 611-618.

[15] F. Abraham, M. Behr and M. Heinkenschloss, Shape optimization in steady blood flow: a numerical study of non-Newtonian effects, *Computer Methods in Biomechanics and Biomedical Engineering*; Vol. 8, No. 2, 2005, pp. 127–137.

[16] M. Probst, M. Lülfesmann, H. Bücker, M. Behr and C.H Bischof, Sensitivity of shear rate in artificial grafts using automatic differentiation, *Int. J. Numer. Meth. Fluids*, Vol. 62, 2010, pp. 1047–1062.

[17] A. Leuprechtt, S. Kozerkee, P. Boeziger and K. Perktold, Blood flow in the human ascending aorta: a combined MRI and CFD study, *J. Eng. Math*., Vol. 47, No. 3, 2003, pp. 387-404.

[18] M.R. Kaazempur-Mofrad, A.G. Isasi, H.F. Younis, R.C. Chan, D.P. Hinton, G. Sukhova, G.M. LaMuraglia, R.T. Lee and R.D. Kamm, Characterization of the Atherosclerotic Carotid Bifurcation Using MRI, Finite Element Modeling and Histology, *Annals of Biomedical Engineering* , Vol. 32, No. 7, 2004, pp. 932-946.

[19] C. Schumann, M. Neugebauer, R. Bade, B. Preim and H.O. Peitgen, Implicit vessel surface reconstruction for visualization and CFD simulation, *Int. J. Computer Assisted Radiology and Surgery*, Vol. 2, 2008, pp. 275–286.

[20] J. Donea and A. Huerta, *Finite Element Methods for Flow Problems*, John Wiley & Sons, England, 2004.

[21] I. Babuska, The finite element method with Lagrangian multipliers, *Numer. Math*., Vol. 20, 1973, pp. 179-192.

[22] F. Brezzi, On the existence, uniqueness and approximation of saddle-point problems ar sing from Lagrangian multipliers, *RAIRO Anal. Numér*, Vol. 8(R2), 1974, pp. 129-151.

[23] I. Babuska, J. Osborn, and J. Pitkaranta, Analysis of mixed methods using, mesh dependent norms, *Math. Comp.*, Vol. 35, 1980, pp. 1039-1062.

[24] G. De Santis, P. Mortier, M. De Beule, P. Segers, P. Verdonck and B. Verhegghe, Patient-specific computational fluid dynamics: structured mesh generation from coronary angiography, *Med. Biol. Eng. Comput.*, Vol. 48, No. 4, 2010, pp. 371-380.

[25] O.C. Zienkiewicz, J.P. Villotte, and S. Toyshima, Iterative method for constrained and mixed approximation - an inexpensive improvement of F.E.M. performance, *Comp. Methd. Appl, Eng.*, Vol. 51, 1985, pp. 3-24.

[26] A.J. Chorin, Numerical solution of the Navier-stokes Equations, *Math. Comp.*, Vol. 22, 1968, pp. 745-762.

[27] O.C. Zienkiewicz, R.L. Taylor and P. Nithiarasu, *The Finite Element Method for Fluid Dynamics*, Elsevier, 2005.

[28] R. Courant, Variational methods for the solution of problems of equilibrium and vibration, *Bull. Amer. Math. Soc.*, Vol. 49, 1943, pp. 1- 23.

[29] D.W. Kelly, S. Nakazawa and O.C. Zienkiewicz, A note on anisotropic balancing dissipation in the finite element method

approximation to convective diffusion problems, *Int. J. for Num. Meth. in Engin*., Vol. 15, 1980, pp. 1705-1711.

[30] T.J.R. Hughes,and A.N. Brooks, A theoretical framework for Petrov-Galerkin methods with discontinuous weighting function, in R.H. Gallagher et al., editors, *Finite Elements in fluids*, Vol. 4, pp. 47-65, John Wiley & Sons, Chichester, 1982.

[31] T.J.R. Hughes, L.P. Franca and M. Balestra, A new finite element method for computational fluid dynamics: V. Circumventing the Babuska-Brezzi condition: A stable Petrov-Galerkin formulation of the Stokes problem accommodating equal order interpolations, *Computer Methods in Applied Mechanics and Engineering*, Vol. 59, 1986, pp. 85-99.

[32] T.J.R. Hughes, L.P. Franca, and G.M. Hulbert, A new finite element method for computational fluid dynamics: VIII The Galerkin/Least Squares method for advective diffusive equations, *Computer Methods in Applied Mechanics and Engineering*, Vol. 73, 1989, pp. 173-189.